First-principles study of LiPON and related solid electrolytes

Yaojun A. Du* and N. A. W. Holzwarth†
Department of Physics, Wake Forest University, Winston-Salem, North Carolina 27109, USA
(Received 12 January 2010; published 13 May 2010)

Lithium phosphorus oxynitride materials have been investigated for many years, especially in relation to the thin-film electrolyte LiPON, developed at Oak Ridge National Laboratory. We have carried out first-principles simulations of related crystalline materials as a first step toward understanding the sources of stability and mechanisms of Li-ion conductivity in these materials. In addition to a comprehensive survey of known crystalline materials related to LiPON, we have also predicted some materials. For example, starting with crystalline $LiPO_3$ which has twisted phosphate chains, we considered the possibility of modifying the structure by substituting N and Li for O. The optimized structures were computed to have regularized phosphate chains which form planar -P-N-P-N- backbones. To the best of our knowledge, the predicted crystals, which we call s_1-Li_2PO_2N with a 24-atom unit cell and s_2-Li_2PO_2N with a 12-atom unit cell, have not yet been observed experimentally. We suggest several possible exothermic reaction pathways to synthesize these crystals.

DOI: 10.1103/PhysRevB.81.184106 PACS number(s): 61.66.Fn, 82.47.Aa, 61.20.Qg, 82.60.Cx

I. INTRODUCTION

The thin-film solid electrolyte LiPON developed at Oak Ridge National Laboratory (ORNL),[1–9] has the composition of $Li_xPO_yN_z$, where $x=2y+3z-5$, and is the most widely used solid electrolyte for thin-film batteries and a number of other related technologies.[10] In addition to studies at ORNL, there has been considerable research[11–14] on the preparation and properties of LiPON materials. However, details of the local stoichiometries and structures responsible for the chemical and mechanical stability and the mechanisms of ionic conductivity are not yet known. While the LiPON materials are disordered, much can be learned from related crystalline materials in the $Li_xPO_yN_z$ family of materials.

A convenient way of systematizing the stoichiometries of the $Li_xPO_yN_z$ family of materials is in terms of a quaternary diagram[15] with vertices at the four constituent compounds—$LiO_{1/2}$, $LiN_{1/3}$, $PO_{5/2}$, and $PN_{5/3}$—as shown in Fig. 1. The number of materials in the family which have been reported in the literature, as indicated by the labels on the edges of the tetrahedron, is quite impressive.

In addition to stoichiometric relationships, the $Li_xPO_yN_z$ family of materials can be categorized in terms of structural patterns. While all of the members of the family have tetrahedral $PO_{4-w}N_w$ building blocks, these can be connected in different ways. For example, they can occur isolated polyatomic ions such as $[PO_4]^{-3}$ in Li_3PO_4 crystals[16] or $[PN_4]^{-7}$ in Li_7PN_4 crystals.[17] Phosphate dimers $[P_2O_7]^{-4}$ have also been observed in $Li_4P_2O_7$ crystals.[18] Alternatively, the phosphate groups can share tetrahedral corner ions making infinitely long chains such as found in $LiPO_3$ crystals.[19,20] More complicated structures, such as multiply connected phosphate network structures such as found in o-$PO_{5/2}$ crystals.[21]

Another meaningful categorization of the $Li_xPO_yN_z$ family of materials is in terms of the placement of N in comparison with O in the various phosphonitride structures. There is considerable literature[22] which suggests that N provides "cross linking" between phosphate chains to provide chemical and mechanical stability to the materials. In addition to the singly coordinated N found in Li_7PN_4, N can be doubly coordinated (connected to two phosphate groups) as found in $LiPN_2$ crystals[23] or can be both doubly and triply coordinated (connected to three phosphate groups) as found in α-P_3N_5,[24] HP_4N_7,[25] and NaP_4N_7.[26]

In this work, we report results of first-principles calculations on many of these materials reported in the literature and additionally some new computer predicted stable and metastable structures. In previous work,[27–29] we focused on properties of the isolated phosphate groups based on Li_3PO_4. In this work, we consider phosphate cluster, chain, and network structures. Four interconnected motivations for undertaking the comprehensive survey of the LiPON family of crystalline materials are (1) to prepare the basis for a study of their electrolyte properties, (2) to provide a quantitative measure of the stability of known as well as predicted members of the family, (3) to take advantage of the large number of experimental results available for members of this family of materials in order to test and refine the validity of the

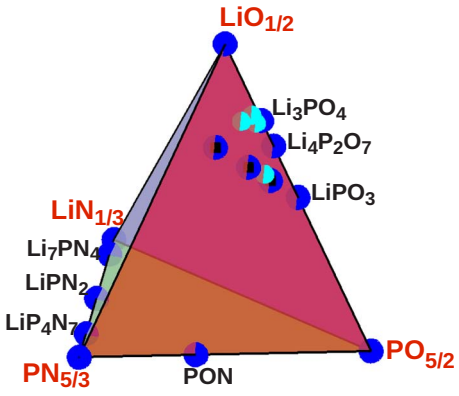

FIG. 1. (Color online) Composition diagram based on $LiO_{1/2}$, $LiN_{1/3}$, $PO_{5/2}$, and $PN_{5/3}$ starting materials. Shown are labeled natural and synthetic crystalline materials [dark (blue) circles]. LiPON thin-film compositions [light (turquoise) circles] reported in the literature and examples of stable and metastable nitrided phosphate materials (■) constructed in this work are also indicated.

calculational models, and (4) to provide a comprehensive resource for further work on the LiPON family of materials for both experimental and theoretical approaches. A fifth motivation for this survey is to provide information which will help identify likely local stoichiometries and structures which may be present in small regions of thin film LiPON electrolytes.

In Sec. II, we discuss the computational methods used in this study. In Sec. III, we present results of our calculated heats of formation for the materials in this study. Detailed structural properties, including lattice parameters, densities of states, and phonon spectra are presented in Sec. IV with separate sections for materials based on phosphate clusters, linear chains of phosphate, and multiply connected phosphate structures in Secs. IV A, IV B, and IV C, respectively. The results are discussed and summarized in Sec. V.

II. CALCULATIONAL METHODS

The calculations performed in this study were based on density-functional theory[30,31] and were primarily carried out using the QUANTUM ESPRESSO (PWSCF) package[32] and the ultrasoft pseudopotential (USPP) formalism of Vanderbilt.[33] The pseudopotentials for Li, P, and O were constructed using the USPP code[33] and tested for agreement with calculations using other methods and codes.[34,35] The form of the exchange-correlation functional was chosen to be the local-density approximation (LDA).[36] Previous work using these techniques gave excellent agreement with experimental studies of the structural properties and phonon spectra of γ-Li_3PO_4.[28] Details of the calculational methods and convergence parameters were the same as in the previous work.[27,28] For convenience, the partial densities of states and charge-density contours were evaluated using the PWPAW code[37,38] which is based on the projector-augmented wave formalism developed by Blöchl.[39] Some energy differences and structural optimizations determined by the PWSCF code were checked using the PWPAW code and also the ABINIT code.[40]

The results of the calculations allow us to predict and analyze stable and metastable structures, estimate heats of formation and phonon vibrational spectra, and to develop qualitative bonding pictures of these materials based on the partial densities of states and electron contour diagrams. These calculations provide the basis for further study of the technologically interesting electrolyte properties of this family of materials.

III. FORMATION ENERGIES

From the total energies of the valence electrons determined from the Kohn-Sham results of all of the materials, we can estimate standard heats of formation. The reference energies, as defined in the CRC Handbook,[41] are solid Li in its body-centered cubic structure, solid P in the "white" structural form, and O_2 and N_2 in their gaseous molecular form. In this work, the reference energy for Li was calculated directly. In order to determine the reference energy for P, we first calculated the energy of the lowest-energy structure—"black" phosphorus which has been determined[42] to have an orthorhombic structure *Cmce* (#64).[43] The energy of white P was determined by adding the experimental value[41] of the heat of formation for white P relative to black P of 39.3 kJ/mol $\equiv$ 0.4073 eV/P. For the molecular reference materials, additional steps had to be taken because, while the Kohn-Sham formalism using the LDA exchange-correlation functional is known to do an excellent job of comparing the energies of materials in the solid state, molecular energies are treated less well. Accordingly, we followed the approach of Wang *et al.*[44] and adjusted our calculated molecular energies of both molecular reference materials O_2 and N_2 by making a least-squares fit to standard heats of formation for the seven compounds indicated in Table I. The fit indicated that the calculated total energies of O_2 and N_2 should be shifted by −0.4159 eV and −1.5356 eV, respectively. With these shifts, the reference energies in electron volt per atom are −194.8150, −355.9719, −435.4027, and −273.5136 for Li, P, O, and N, respectively. Of course these numbers are dependent on internal energy references within the calculation scheme. On the other hand, energy differences are reliable and have been checked using several codes as discussed above.

While all calculations are based on results for idealized crystals corresponding to experimental temperatures of 0 K, we estimate that the additional heat and work needed to bring the materials to the standard temperature of 298.15 K is negligible compared to the overall error of the calculational methods. The results of our calculations of the total energies of all of the materials of this study, including the materials used in the fit are given in Table I. The calculated results agree with the available experimental results within 0.4 eV. It is expected that relative energies between structurally and chemically similar materials are considerably more accurate than the overall error.

The results shown in Table I show interesting relationships. Among the $Li_xPO_yN_z$ family members, the highest formation energy per P is found in Li_3PO_4 which is characterized by isolated $[PO_4]^{-3}$ polyions. The next highest formation energy per P is found in $Li_2PO_{7/2}$ which is characterized by isolated phosphate dimers $[P_2O_7]^{-4}$.[18] The third highest formation energy per P is found in the phosphate chain structure $LiPO_3$ in which each phosphate tetrahedron is connected to two others forming an infinite chain. The experimentally determined structure ($P2/c$ #13) (Ref. 20) has a slightly lower formation energy than any of the simpler structures found in our computer simulations. While there is not a one-to-one structural correspondence between the oxide (Li_xPO_y) and nitride (Li_xPN_z) materials, it is generally the case that the oxide materials have a lower formation energy than the nitrides. Intriguing new materials with the stoichiometry Li_2PO_2N were found in several high-symmetry structures as will be discussed below.

One would hope that the calculated formations are accurate enough to estimate heats of reaction. We have listed several observed reactions and our estimate of their exothermic energy release in Table II. In making these estimates, when there was some ambiguity in the form of the starting materials, we chose the more stable materials. While this is

TABLE I. Summary of optimization results for $Li_xPO_yN_z$ and related materials. For each formula unit (given in first column of the table), the space-group symbol and (number) (Ref. 43) is listed in the second column. The calculated heat of formation ΔH in units of electron volts per formula unit is given in the third column and compared with (experimental values) when available. Experimental values indicated with "*" were used fitting the O_2 and N_2 reference energies as explained in the text. The calculated volume per formula unit $\mathcal{V}$ in units of Å^3 is given in the fourth column and compared with (experimental values) when available.

Material	Structure	ΔH	$\mathcal{V}$
Li_2O	$Fm\bar{3}m$ (#225)	−6.13 (−6.20* [a])	
α-Li_3N	$P6/mmm$ (#191)	−1.59 (−1.71* [b])	
$LiNO_3$	$R\bar{3}c$ (#167)[i]	−5.43 (−5.01* [a])	
h-$PO_{5/2}$	$R3c$ (#161)[j]	−7.74 (−7.73* [c])	46 (52)
o-$PO_{5/2}$	$Fdd2$ (#43)[k]	−7.91 (−7.88 [d])	42 (44)
α-$PN_{5/3}$	$C2/c$ (#15)[l]	−1.07 (−1.11* [b])	33 (33)
PON	$I\bar{4}2d$ (#122)[m]	−4.03 (−3.85* [e])	37 (37)
Li_7PN_4	$P\bar{4}3n$ (#219)[n]	−9.69	97 (103)
$LiPN_2$	$I\bar{4}2d$ (#122)[o]	−3.70	36 (37)
$Li_{1/4}PN_{7/4}$	$P2_1/c$ (#14) [f,p]	−1.79	32
$Li_{1/4}PN_{7/4}$	$C2/c$ (#15)[g,q]	−1.78	30
γ-Li_3PO_4	$Pnma$ (#62)[r]	−21.28 (−21.72* [a])	75 (79)
$Li_2PO_{7/2}$	$P\bar{1}$ (#2)[s]	−17.05	68 (71)
$Li_{5/2}PO_3N_{1/2}$	$P\bar{1}$(#2)[h]	−16.67	68
$LiPO_3$	$P2/c$ (#13)[t]	−12.80	56 (57)
s_1-$LiPO_3$	$Pbcm$ (#57)[h]	−12.73	58
s_2-$LiPO_3$	$Aem2$ (#39)[h]	−12.73	58
s_3-$LiPO_3$	$Pmc2_1$ (#26)[h]	−12.70	67
s_1-Li_2PO_2N	$Pbcm$ (#57)[h]	−12.42	57
s_2-Li_2PO_2N	$Aem2$ (#39)[h]	−12.45	57
s_3-Li_2PO_2N	$Pmc2_1$ (#26)[h]	−12.08	66

[a]From CRC Handbook (Ref. 41).
[b]From NIST website (Ref. 45).
[c]From Ref. 46.
[d]From Ref. 47.
[e]From Ref. 48; calculated value corresponds to lowest energy configuration of disordered N and O sites.
[f]Optimized structure based on structure of HP_4P_7.
[g]Optimized structure based on structure of NaP_4P_7.
[h]Optimized structure found in this work.
[i]Reference 49.
[j]Reference 50.
[k]Reference 21.
[l]Reference 24.
[m]Reference 51.
[n]Reference 17.
[o]References 23 and 52.
[p]Reference 25.
[q]Reference 26.
[r]Reference 16.
[s]Reference 18.
[t]Reference 20.

TABLE II. Some predicted reactions from first-principles calculations. The first column indicates the reaction. The second column gives the exothermic energy release (ΔH in electron volts for given stoichiometry) estimated by our calculations. The last column gives a literature reference where the reaction was mentioned.

Reaction	ΔH	Reference
$7Li_3N+P_3N_5 \rightarrow 3Li_7PN_4$	14.8	17
$Li_3N+P_3N_5 \rightarrow 3LiPN_2$	6.3	23
$Li_2O+P_2O_5 \rightarrow 2LiPO_3$	3.6	53
$P_2O_5+P_3N_5 \rightarrow PON$	1.1	54

not a quantitative comparison, it is encouraging and provides some confidence for the prediction of new reaction discussed further below.

In order to make a qualitative correlation of the formation-energy trends with the structural properties, we list in Table I the experimental and calculated volume per formula unit for members of the LiPON family of materials. As expected for calculations using the LDA exchange-correlation functional, the volumes are systematically calculated to be smaller than experiment but close enough to see the qualitative trends. The largest volume per P is found in materials with isolated tetrahedral—Li_3PO_4 and Li_7PN_4. The next largest volume per P is found in the material with isolated phosphate dimmers—$Li_2PO_{7/2}$ which is discussed in more detail in Sec. IV A below. The chain structure materials $LiPO_3$ have a considerably smaller volume per P than either of these classes of materials. The volume for experimentally realized structure[20] (56–57 Å^3) is smaller than the computer generated structures (58–67 Å^3). These structures are discussed in more detail in Sec. IV B. The most compact structures in this family are found with multiply connected phosphate and phosphonitride groups as discussed in more detail in Sec. IV C.

IV. DETAILED RESULTS

A. Phosphate clusters

1. Structural forms

Crystals of Li_3PO_4 in γ and β structures are based on isolated PO_4^{-3} ions. As has been discussed in previous work,[27–29] the two structures are very similar in terms of their total energies and their packing volumes; differing primarily in the relative orientations of the phosphate tetrahedra.

Crystals of $Li_4P_2O_7$ are based on phosphate dimers where two phosphate groups share a "bridging" O. This material has been found[18] to crystallize in the $P\bar{1}$ structure with 26 atoms per unit cell. Figure 2 shows a ball and stick diagram of the structure indicating the relative alignment of the dimers.

The optimized structure determined in the calculation is in very good agreement with the single crystal x-ray results reported in Ref. 18 as shown in the quantitative results given in Table III. The calculated values of the lattice parameters

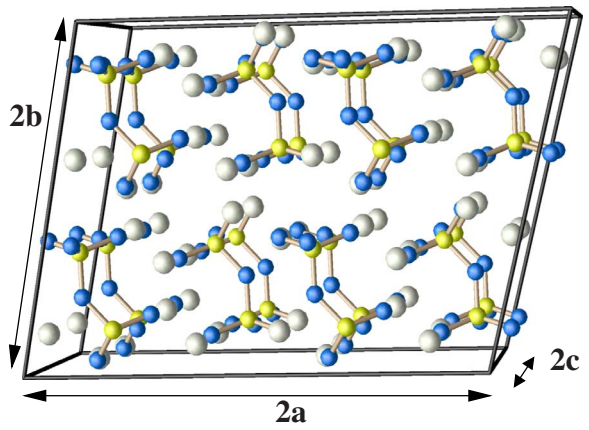

FIG. 2. (Color online) Ball and stick diagram of eight unit cells of $Li_4P_2O_7$ in the $P\bar{1}$ structure (using a nonstandard origin). The atomic sites are indicated with the following ball styles: Li (light), P [gray (yellow)], and O [dark (blue)].

are systematically smaller than experiment as is consistent with previous experiences with LDA calculations. The comparison between calculated and measured fractional coordinates generally shows a difference smaller than ± 0.01 fractional units.

TABLE III. Top table lists lattice parameters (in Å) and angles (in degrees) for $Li_4P_2O_7$ in the $P\bar{1}$ structure, comparing experimental results of Ref. 18 with calculations of the original and nitrided materials. Second table lists inequivalent fractional coordinates of a conventional cell of $Li_4P_2O_7$ comparing computed and (experimental values).

	a	b	c	α (deg)	β (deg)	γ (deg)
$Li_4P_2O_7$ (expt.)	8.56	7.11	5.19	111.4	90.0	103.1
$Li_4P_2O_7$ (calc.)	8.40	7.01	5.13	111.7	90.0	103.6
$Li_5P_2O_6N$ (calc.)	8.46	7.20	4.86	109.9	90.3	100.2

Atom	x	y	z
P(1)	0.850 (0.846)	0.227 (0.222)	0.444 (0.438)
P(2)	0.626 (0.631)	−0.216(−0.214)	0.215 (0.214)
O(1)	0.680 (0.684)	0.042 (0.038)	0.315 (0.308)
O(2)	0.882 (0.875)	0.268 (0.259)	0.752 (0.741)
O(3)	0.798 (0.794)	0.407 (0.398)	0.394 (0.390)
O(4)	0.985 (0.982)	0.149 (0.151)	0.268 (0.270)
O(5)	0.618 (0.622)	−0.264(−0.261)	0.482 (0.476)
O(6)	0.463 (0.472)	−0.276(−0.270)	0.045 (0.047)
O(7)	0.763 (0.763)	−0.296(−0.297)	0.041 (0.041)
Li(1)	0.788 (0.791)	0.677 (0.673)	0.653 (0.644)
Li(2)	0.444 (0.452)	0.745 (0.755)	0.699 (0.702)
Li(3)	0.763 (0.754)	0.422 (0.412)	0.027 (0.016)
Li(4)	0.987 (0.988)	0.855 (0.854)	0.106 (0.110)

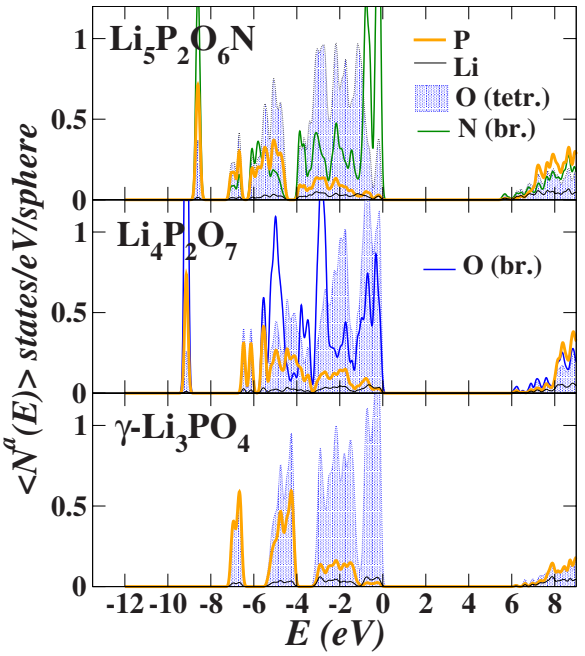

FIG. 3. (Color online) Partial densities of states plots for $Li_4P_2O_7$ and $Li_5P_2O_6N$ in the $P\bar{1}$ structure compared with that of γ-Li_3PO_4. The abbreviations "tetr." and "br." are used to distinguish sites with tetrahedral and bridge bond coordination of O or N with neighboring P, respectively.

In addition to considering the reported material, we also considered the possibility of introducing N into this structure. From past experience,[27] we know that it is energetically favorable for N to substitute for an O in a bridging site between two phosphate groups (or corner sharing site) rather than an tetrahedral site. If every bridging O were replaced by N (plus Li to ensure charge neutrality), the stoichiometry would be $Li_5P_2O_6N$. Of the several possible structures of this material which maintain the $P\bar{1}$ structure, the lowest-energy structure reported in Table I has the lattice parameters given in Table III and its inequivalent atom positions are given in Table XII in the Appendix. We did verify that if the N's were to have replaced tetrahedral O's instead of the bridging O's, the total energy per formula unit was higher than that reported in Table I by at least 1.7 eV. The optimized structure of $Li_5P_2O_6N$ is very close to that of $Li_4P_2O_7$ as shown in Table XII. The extra Li sites are positioned 2.0 Å from a N site in a dimer and 1.9 Å from two O sites in an adjacent dimer.

2. Densities of states

The partial densities of states of these materials contain useful qualitative information about covalent bonding properties. Using Eq. 1 of Ref. 28, we have evaluated the partial densities of states for $Li_4P_2O_7$ and $Li_5P_2O_6N$ and compared them with those of Li_3PO_4 in the γ structure as shown in Fig. 3. Each plot of $\langle N^a(E)\rangle$ represents the density of states weighted by the charge within each atomic sphere a, averaged over spheres of each atom type. The pattern of the partial densities of states for both $Li_4P_2O_7$ and $Li_5P_2O_6N$ are

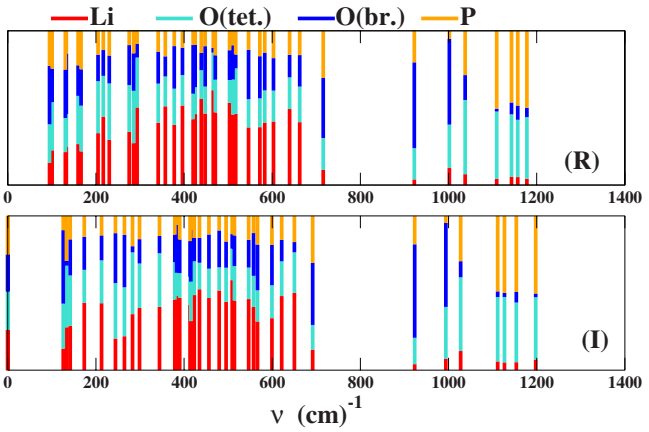

FIG. 4. (Color online) Raman-active (R) and infrared-active (I) zone-center lattice vibrations (in units of per centimeter) for $Li_4P_2O_7$. The lengths of the lines segments indicate the contribution of each atomic type as defined in Eq. (1). In this case, we distinguish the O sites having a tetrahedral configuration to P by "O (tet.)" and the O sites associated with the bridge bonds by "O (br.)."

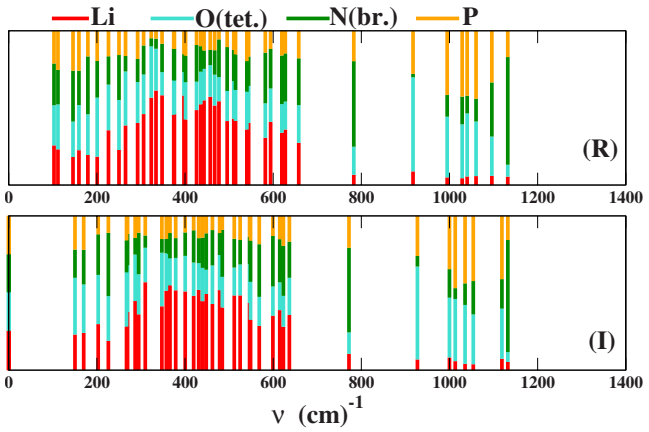

FIG. 5. (Color online) Raman-active (R) and infrared-active (I) zone-center lattice vibrations (in units of per centimeter) for $Li_5P_2O_6N$ plotted in the same scheme as in Fig. 4 except that bridge bonds are occupied by N's and the amplitudes are labeled "N (br.)."

very similar; the bridging O contributions are at lower energy than those of the bridging N, as expected from the greater nuclear attraction of O compared to that of N. Both materials have a low-energy state of $2p\sigma$ character associated with the bridging O or N ion, similar to that previously identified in PNP and POP defect structures in Li_3PO_4 crystals.[27] Presumably these states contribute to the stability of the dimer structures.

3. Lattice vibrations

The zone-center vibrational modes including both infrared- and Raman-active modes were calculated. In analyzing the phonon spectra of the materials, we developed the following method for qualitative interpretation of the modes. For the equilibrium configuration of the system with atomic positions $\{\mathbf{R}_0^a\}$, where a indexes the atomic sites, the QUANTUM ESPRESSO package determines the dynamical matrix and solves for the normal-mode displacements $\{\delta\mathbf{R}^a\}$ for all atoms in the unit cell. In general, we are interested in the magnitudes of the displacements of each type of atom in order to distinguish Li-ion motions from those of P, O, and N. Accordingly, we can define an average displacement for each type of atom according to

$$\langle|\delta\mathbf{R}^t|\rangle \equiv \frac{1}{N_t}\sum_{a\in t}|\delta\mathbf{R}^a|, \tag{1}$$

where the sum is taken over the N_t sites in the unit cell corresponding to atom type $a=t$. For plotting purposes these average displacements $\langle|\delta\mathbf{R}^t|\rangle$ are then scaled to unity.

Results for $Li_4P_2O_7$ are presented in Fig. 4. This spectrum has some similarity to the phonon spectra of Li_3PO_4 presented in Ref. 28. There is a gap in the spectrum between $720 \leq \nu \leq 910$ cm^{-1}. The highest-frequency mode is 1200 cm^{-1} while for Li_3PO_4, the highest-frequency mode is 1150 cm^{-1}. Modes with the largest involvement of the bridging O occur at 920 and 1000 cm^{-1}. The modes with the largest involvement of Li motion occur at frequencies $0 \leq \nu \leq 700$ cm^{-1}. We will see that this pattern is common to this family of materials. Results for our structure of $Li_5P_2O_6N$ are presented in Fig. 5. The spectrum covers a slightly smaller frequency range than that of $Li_4P_2O_7$ and the modes with the largest involvement of bridging N motions occur at 780 and 1130 cm^{-1}.

B. Linear phosphate chains

1. Structural forms

Crystals of $LiPO_3$ are characterized by infinite linear chains of phosphate, where in each formula unit, two O's make tetrahedral bonds with P while the third O is involved with a bridge bond between two phosphate groups. $LiPO_3$ can be prepared from a Li_2O-P_2O_5 glass by heating to the crystallization temperature of 486 °C.[53] The structure of crystalline $LiPO_3$ was analyzed by Murashova and Chudinova.[20] It was found to have the space group $P2/c$ (#13 in the *International Tables of Crystallography*) (Ref. 43) with 100 atoms per primitive unit cell. Earlier structural analysis by Guitel and Tordjman[19] is equivalent. Figure 6

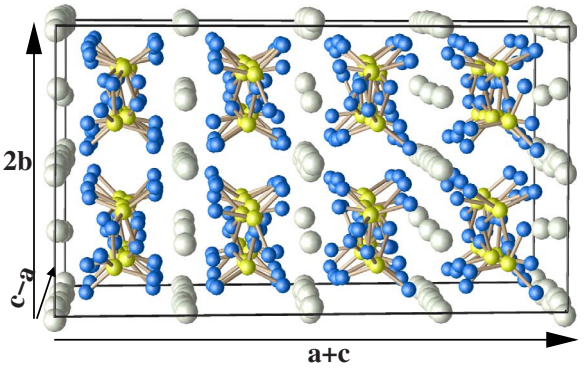

FIG. 6. (Color online) Ball and stick model of natural $LiPO_3$ using the same ball styles as given in Fig. 2. The chain direction is perpendicular to the plane of the diagram.

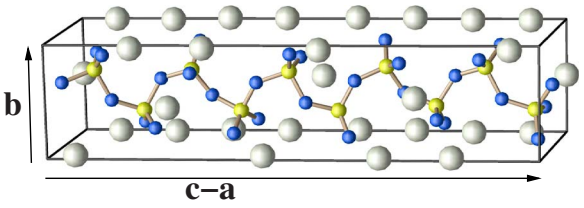

FIG. 7. (Color online) Single chain view of natural $LiPO_3$ shown in Fig. 6.

shows a ball and stick model of the structure, showing the arrangement of the chains using lattice parameter labels consistent with Ref. 20. It is also helpful to visualize the chain structure itself shown in Fig. 7. This figure shows the chain to be twisted about its axis with a periodicity of ten phosphate groups.

Table IV shows the comparison between the calculated and experimental lattice parameters while the calculated and measured fractional coordinates are given in Table XIII in the Appendix. Again, the agreement between experiment and calculation is quite good.

In addition to studying this naturally occurring structure, we constructed several related stable and metastable structures, primarily motivated by the question of the role of N in the LiPON materials.

First, we considered the possibility of substituting N for O in natural $LiPO_3$. From past experience[27] including the study of $Li_5P_2O_6N$ described above, we know that it is energetically favorable for N to substitute for an O in a bridging site between two phosphate groups (or corner-sharing site) rather than an tetrahedral site. Therefore, starting with the $P2/c$ structure of natural $LiPO_3$, we substituted the 20 bridging oxygen with nitrogen and also introduced 20 additional Li atoms into the structure. The relaxation results were remarkable; showing that the nitrided chain has a very stable structure with a periodicity of $(PO_2N)_2$ groups. The optimized structure (which we call s_1-Li_2PO_2N) was found to have 24 atoms per unit cell with *Pbcm* symmetry (#57). The most intriguing structural feature of s_1-Li_2PO_2N compared to $LiPO_3$ in its natural monoclinic $P2/c$ structure, is the regularization of the chain structure with a planar -P-N-P-N- backbone.

In the s_1-Li_2PO_2N structure, there are two orientationally inequivalent phosphonitride chains. If one of the chains is rotated by 180° about a perpendicular axis, the s_2-Li_2PO_2N structure is obtained. This second structure has 12 atoms per unit cell with *Aem*2 (#39) symmetry. As shown in Table I, the energies and volumes of these two structures are very similar. Once these two new compounds were obtained, we found corresponding metastable structures of

TABLE IV. Lattice parameters (in Å) for the $P2/c$ structure of $LiPO_3$ comparing calculated results with the experimental results of Ref. 20.

	a	b	c	β (deg)
Expt.	13.074	5.4068	16.452	99.00
Calc.	13.00	5.30	16.31	98.8

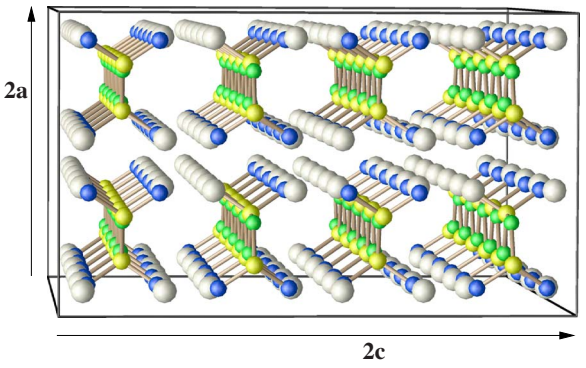

FIG. 8. (Color online) Ball and stick model of s_1-Li_2PO_2N structure using same ball styles as in Fig. 2 with the addition of N [dark gray (green)].

$LiPO_3$—s_1-$LiPO_3$ and s_2-$LiPO_3$ with *Pbcm* and *Aem*2 symmetries, respectively. Figures 8 and 9 show several unit cells of *Pbcm* crystals for s_1-Li_2PO_2N and s_1-$LiPO_3$, respectively, in a similar perspective as the natural structure shown in Fig. 6. More detail of the chain structures are shown in Fig. 10 which also shows charge-density contours in the plane of the chains. The chain structure of s_1-$LiPO_3$ shown in Fig. 10 is clearly a regularized version of the chain structure in the natural $LiPO_3$ shown in Fig. 7, with a strict planar structure for the backbone P-O-P groups. Since the energy of this structure is 0.06 eV higher than that of natural $LiPO_3$, it is unlikely that it could be physically realized. However, it is a useful structure as an idealized model of the natural structure and perhaps short sections of the glass. The chain structure of the corresponding *Aem*2 structures is virtually identical to those of the *Pbcm* structures. The s_1-$LiPO_3$ and s_2-$LiPO_3$ structures provide useful references for their nitrided counter parts—s_1-Li_2PO_2N and s_2-Li_2PO_2N, which we predict to be physically realizable materials. The s_1-Li_2PO_2N chain structure shown in Fig. 10 has a very similar backbone structure with a strict planar structure for the backbone P-N-P groups. The main difference is that while in s_1-$LiPO_3$, the Li's are shared between tetrahedral O's in different chains, s_1-Li_2PO_2N has one Li for every tetrahedral O. In fact, in both s_1-Li_2PO_2N and s_2-Li_2PO_2N structures, each Li has both N and O nearest neighbors. The electron charge-density contours in the backbone planes of Fig. 10 show that in the P-N-P structure the density is more dispersed than in the

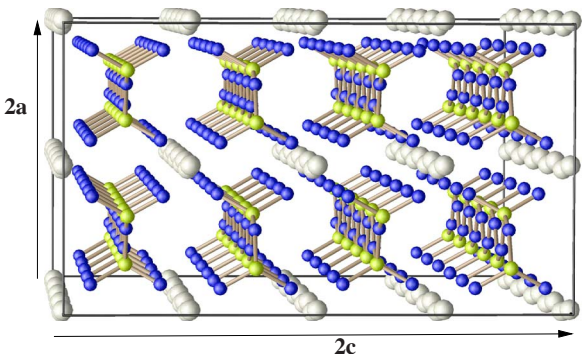

FIG. 9. (Color online) Ball and stick model of s_1-$LiPO_3$ structure using same ball styles as in Fig. 2.

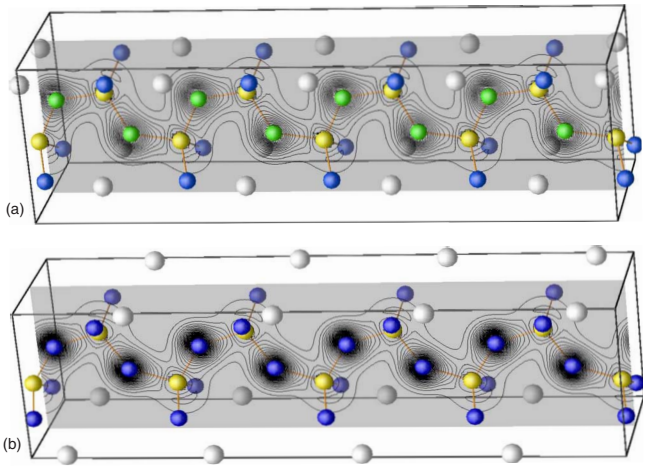

FIG. 10. (Color online) Single chain views of s_1-Li_2PO_2N (a) and s_1-$LiPO_3$ (b) with superimposed contours of valence densities plotted in a plane passing through each chain.

corresponding P-O-P structure. A similar trend was seen in previous work[27] on dimer P-N-P and P-O-P structures.

Table V lists the lattice parameters and inequivalent fractional coordinates for the four materials. The primitive unit cells of the *Aem*2 structured materials contain half as many atoms as the corresponding *Pbcm* structured materials. These tables quantify that for each crystal type, the phosphate chain structures found in Li_2PO_2N and $LiPO_3$ materials are very similar.

There are many other metastable structures of the phosphonitride chain materials. For example, we were able to construct a so-named s_3-Li_2PO_2N with $Pmc2_1$ (#26) symmetry in the following way. Our previous studies of O and N defects in γ-Li_3PO_4 showed that if one O is removed and another O is replaced by N in a given PO_4 group, it is possible to form phosphate dimers with P-N-P bonds. Starting with a supercell of γ-Li_3PO_4, we were able to form a metastable structure with periodic P-N-P chain structure by systemically removing one O, removing one Li, and substituting one O with N for each formula unit, with several intermediate optimization steps. As reported in Table I, the resulting s_3-Li_2PO_2N structure has an energy 0.35 eV higher than that of s_1-Li_2PO_2N and the corresponding s_3-$LiPO_3$ structure has an energy 0.03 eV higher than that of s_1-$LiPO_3$. Figure 11 presents a ball and stick model of the nitrided structure. This structure has 24 atoms in the primitive unit cell and its chains are characterized by a repeat unit of $(PO_2N)_2$ but in contrast to the s_1 and s_2 structures, the phosphate groups within a repeat unit are twisted by 90° relative to each other. This structure is also characterized by greater void spaces than the other structures.

The optimized lattice constants for both s_3-Li_2PO_2N and s_3-$LiPO_3$ are given in Table VI and the corresponding fractional coordinates are in Table XIV given in the Appendix. While it may not be possible for these structures to be physically realized, they also are good examples of idealized chain structures which may represent local geometries in glass phase materials. They also clearly demonstrate the flexibility of the phosphate chain geometries.

TABLE V. Top table lists computed lattice parameters (in Å) for the *Pbcm* structures of s_1-Li_2PO_2N and s_1-$LiPO_3$ and the *Aem*2 structures of s_2-Li_2PO_2N and s_2-$LiPO_3$. Second table lists computed inequivalent fractional coordinates in conventional cells of these crystals. The "Pos" column indicates the conventional cell multiplicity and Wyckoff label (Ref. 43).

	a	*b*	*c*
s_1-Li_2PO_2N	5.35	4.68	9.16
s_1-$LiPO_3$	5.27	4.73	9.28
s_2-Li_2PO_2N	5.35	9.08	4.68
s_2-$LiPO_3$	5.29	9.28	4.75

Atom	Pos	*x*	*y*	*z*
		s_1-Li_2PO_2N		
Li	8*e*	0.167	−0.454	−0.408
P	4*d*	0.341	0.456	0.250
O	8*e*	0.184	−0.039	−0.386
N	4*d*	−0.387	−0.388	0.250
		s_1-$LiPO_3$		
Li	4*c*	−0.021	0.250	0.000
P	4*d*	0.323	0.438	0.250
O(1)	8*e*	0.185	0.014	−0.388
O(2)	4*d*	−0.421	−0.383	0.250
		s_2-Li_2PO_2N		
Li	8*d*	0.168	0.409	−0.049
P	4*c*	0.341	−0.250	−0.043
O	8*d*	0.185	−0.113	0.040
N	4*c*	−0.387	−0.250	0.113
		s_2-$LiPO_3$		
Li	4*a*	0.000	0.000	0.219
P	4*c*	0.323	−0.250	−0.076
O(1)	8*d*	0.185	−0.112	−0.029
O(2)	4*c*	−0.423	−0.250	0.106

2. Densities of states

The partial densities of states of these materials contain useful qualitative information about covalent bonding properties. Figure 12 compares the partial densities of states of three forms of the phosphate chain materials. (The partial densities of states of s_1-$LiPO_3$ and s_2-$LiPO_3$ are nearly iden-

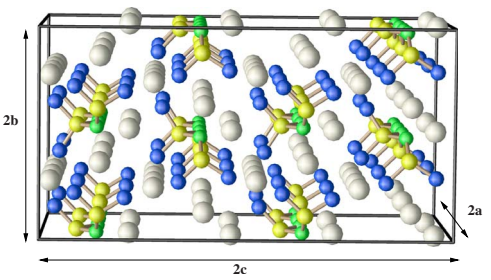

FIG. 11. (Color online) Ball and stick model of s_3-Li_2PO_2N structure using same ball styles as in Fig. 8.

TABLE VI. Computed lattice parameters (in Å) for the $Pmc2_1$ structures of s_3-Li_2PO_2N and s_3-$LiPO_3$.

	a	b	c
s_3-Li_2PO_2N	5.13	5.14	10.04
s_3-$LiPO_3$	4.97	5.36	10.12

tical so only one is presented.) From these plots, it is evident that the low-energy $2p\sigma$ state associated with the P-O-P bridge bonds found in the dimer material $Li_4P_2O_7$ has now become a one-dimensional band. (In fact, the spiky structure seen in these plots is due to the sensitivity of the density of states to the k-point sampling of one-dimensional bands.) These σ-bond chain bands have a width of approximately 3 eV and they are separated from the main contributions of the tetrahedral O states by approximately 2 eV. Because of these low-energy σ-bond bands, the overall valence bandwidth of the $LiPO_3$ materials is considerably larger than that of γ-Li_3PO_4.

The partial densities of states of two structural forms of Li_2PO_2N are shown in Fig. 13. The qualitative features of the plots are quite similar to those of the corresponding $LiPO_3$ materials, although the states due to N are generally shifted to higher-energy relative to those of O. The low-energy σ bands associated with the P-N-P chains have a bandwidth of roughly 3 eV and are located just below the main contributions due to the tetrahedral oxygen. In both of the structures, the highest occupied states correspond to the upper π bands on the N sites. Further analysis of the s_1-Li_2PO_2N structure indicates that these states have most of their density perpendicular to the plane of the chains, consistent with the notion of "lone-pair" states[55] of N.

3. Lattice vibrations

In order to further evaluate the lattice properties of these materials, we also calculated the zone-center lattice vibrations. Figure 14 shows both the Raman-active and infrared active modes of s_1-Li_2PO_2N while Figs. 15 and 16 give the corresponding plots for s_1-$LiPO_3$ and natural $LiPO_3$, respectively.

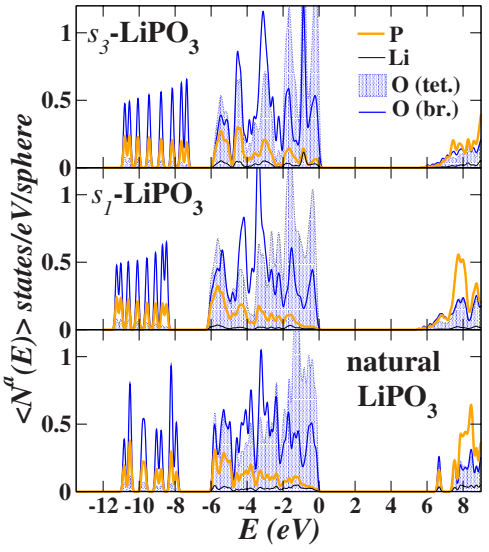

FIG. 12. (Color online) Partial densities of states plots for natural $LiPO_3$, s_1-$LiPO_3$, and s_3-$LiPO_3$ using the same notation as in Fig. 3.

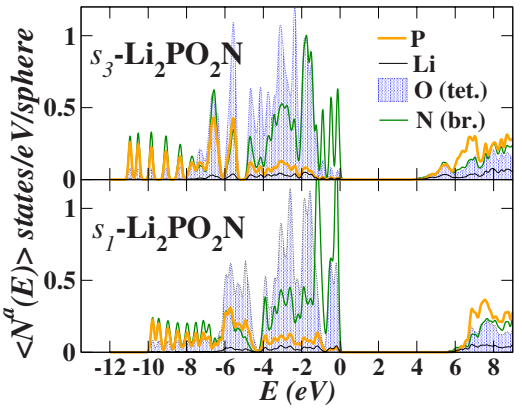

FIG. 13. (Color online) Partial densities of states plots for s_1-Li_2PO_2N, and s_3-Li_2PO_2N using the same notation as in Fig. 3.

In general, the vibrational modes for the nitrided crystal are at lower frequency than the corresponding modes for the pure phosphate crystals. The highest frequency for the $LiPO_3$ structures is 1350 $(cm)^{-1}$ while for s_1-Li_2PO_2N, it is 1130 $(cm)^{-1}$. We see that the main involvement of Li motions comes in the lower-frequency modes in the range $0 \leq \nu \leq 700$ $(cm)^{-1}$, which couple to local rotations of the phosphonitride tetrahedra. Not surprisingly, there is a much denser distribution of those modes in natural $LiPO_3$, than for the simpler s_1-$LiPO_3$ structure. The modes corresponding to stretching vibrations of the tetrahedral P-O bonds are the highest-frequency modes $1100 \leq \nu \leq 1350$ $(cm)^{-1}$ in the $LiPO_3$ materials. For s_1-Li_2PO_2N, the corresponding modes occur in the lowered-frequency range $960 \leq \nu \leq 1130$ $(cm)^{-1}$. Modes that have significant involvement of the bridging N occur at the frequencies 850, 1060, and 1120 $(cm)^{-1}$ for s_1-Li_2PO_2N. The corresponding bridge bond O modes occur at the frequencies 940 and 1070 $(cm)^{-1}$ for s_1-$LiPO_3$ and in a similar range for natural $LiPO_3$. There are similarities between the vibrational modes of the infinite

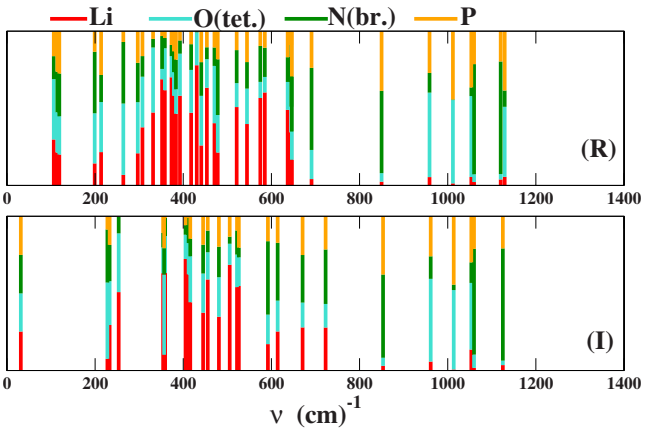

FIG. 14. (Color online) Raman-active (R) and infrared-active (I) zone-center lattice vibrations for s_1-Li_2PO_2N using the same notation as that given in Fig. 5.

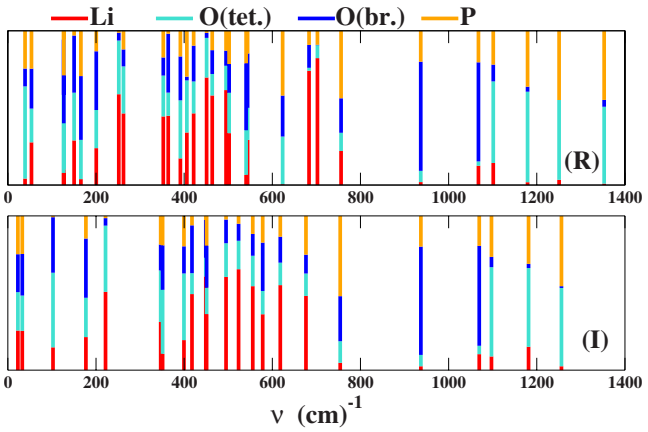

FIG. 15. (Color online) Raman-active (R) and infrared-active (I) zone-center lattice vibrations for s_1-$LiPO_3$ using the same notation as that given in Fig. 4.

chain structures s_1-Li_2PO_2N and s_1-$LiPO_3$ shown in Figs. 14 and 15 and the corresponding dimer materials $Li_5P_2O_6N$ and $Li_4P_2O_7$ in Figs. 5 and 4, respectively.

C. Network structure materials

1. Structural forms

The next level of complication for the phosphate structures can be described in terms of "networks" of phosphate groups connected in multiple dimensions and multiple bonding configurations. An example of a network structure materials is o-P_2O_5 which has been crystallized in the *Fdd*2 structure.[21] The primitive cell has 14 atoms. Figure 17 shows the conventional cell structure. Each PO_4 group is connected to three other PO_4's through bridging O sites, leaving 1 isolated tetrahedral O for each phosphate.

Table VII compares the calculated and experimental lattice parameters and fractional coordinates, respectively, generally showing very good agreement.

Another example of a network structured material is α-P_3N_5 which has the $C2/c$ structure.[24,56] It is one of the most densely packed materials with respect to the volume per P as indicated in Table I characterized with both doubly and triply coordinated N's. The primitive unit cell contains 16 atoms. A ball and stick diagram of the conventional unit cell is given in Fig. 18.

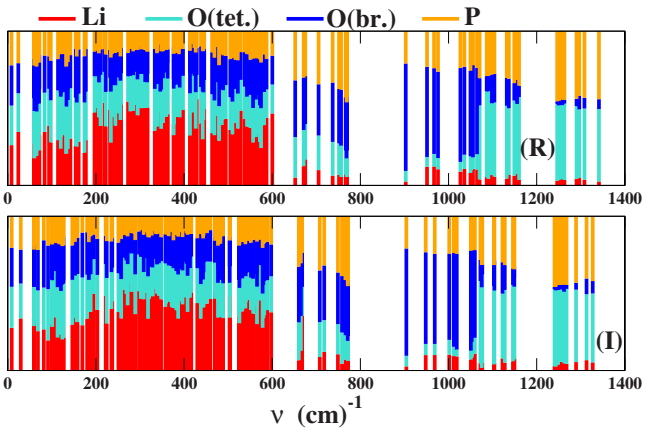

FIG. 16. (Color online) Raman-active (R) and infrared-active (I) zone-center lattice vibrations for natural $LiPO_3$ using the same notation as that given in Fig. 4.

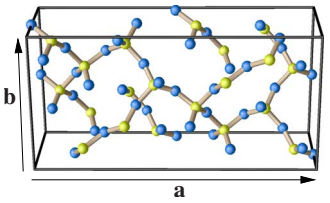

FIG. 17. (Color online) Ball and stick model of conventional unit cell o-P_2O_5 in its *Fdd*2 structure using ball styles of previous figures.

Table VIII lists the lattice constants and fractional coordinates in comparison with experiment. In this notation,[24] the triply coordinated N site is labeled N(3). The structural parameters from our calculations are in good agreement with both experiment and the previous computational results of Kroll and Schnick[56] and Dong *et al.*[57] Interestingly, our computed lattice constants for α-P_3N_5 are slightly larger than experimental and previous calculational results. Since this trend is unusual for LDA calculations of this type, the result was rechecked using both the PWSCF and ABINIT codes.

An example of a network structure which also contains Li is $LiPN_2$ which has been crystallized in the $I\bar{4}2d$ (#122) structure.[23,52] In this structure, each P is bonded to four bridging N's. The primitive cell has eight atoms and contains three inequivalent sites (one for each atom type) as shown in Fig. 19. In Table IX, the calculated and experimental lattice parameters are compared. Our calculated results are very similar to those recently reported by Basalaev *et al.*[58]

As far as we know, no other Li-containing network structures have been reported. However, based on reported structures for HP_4PN_7 ($P2_1/c$, Ref. 25) and NaP_4PN_7 ($C2/c$ Ref. 26), we have found two metastable structures for LiP_4PN_7 which are shown in Fig. 20. These structures are closely packed and the nitrogens have multiple bonding configura-

TABLE VII. Top table lists lattice parameters (in Å) for the *Fdd*2 structure of o-P_2O_5 comparing calculated results with the experimental results of Ref. 21. Second table lists computed inequivalent fractional coordinates for a conventional cell of this crystal compared with the (experimental values).

	a	*b*	*c*
Expt.	16.314	8.115	5.265
Calc.	16.29	8.13	5.12

Atom	Pos	*x*	*y*	*z*
P	16*b*	0.176 (0.175)	0.165 (0.169)	–0.001 (0.000)
O(1)	16*b*	0.197 (0.194)	0.083 (0.085)	0.244 (0.234)
O(2)	16*b*	0.112 (0.113)	0.311 (0.320)	0.021 (0.026)
O(3)	8*a*	0.250 (0.250)	0.250 (0.250)	0.848 (0.857)

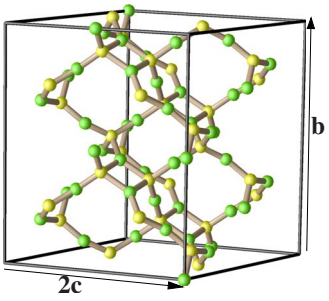

FIG. 18. (Color online) Ball and stick model of conventional unit cell of α-P_3N_5 in the $C2/c$ structure using the ball styles given in previous diagrams.

tions. A comparison of the calculated and experimental lattice parameters is given in Table X. Fraction atomic positions are given in the Tables XV and XVI in the Appendix.

2. Densities of states

It is interesting to compare the densities of states of some of these network structured materials which are shown in Fig. 21. From these results, we see that the bandwidths for these structures are considerably larger than those of the isolated clusters and of the linear chain materials. The triply coordinated N states in α-P_3N_5 and in LiP_4N_7 contribute throughout the spectrum, having larger contributions in the lower-energy range where N $2p\sigma$ bridge bond states also contribute. Our density of states for $LiPN_2$ are in good agreement with the previously reported results of Basalaev *et al.*[58] In all of these density of states plots, there is a separation between the upper states having mostly N or O $2p\pi$ character and the lower-energy states having mostly N or O $2p\sigma$ character. The bandwidth for the O $2p\pi$ states in o-P_2O_5 is larger roughly 2 eV larger than the corresponding bandwidths for the N $2p\pi$ states in the phosphorus nitride materials.

3. Lattice vibrations

Figures 22–25 show the analyzed zone-center vibrational spectral for the network structure materials. To the best of our knowledge, the only experimental measurement to which we can compare these results is the infrared spectrum of α-P_3N_5 which has been measured by several groups.[24,56,59] In Fig. 26, we show the results of our infrared-active frequency modes superposed on the experimental measurements of Horstmann *et al.*,[24] showing excellent agreement especially in the range of the highest-frequency modes at $\nu = 1410$ cm^{-1}. Early calculations on this same system by Kroll *et al.*[56,60] were also in reasonable agreement with experiment, although in that work the highest modes were calculated to be 50 cm^{-1} lower than those measured experimentally. For $LiPN_2$, the vibrational spectrum was also calculated in the earlier work of Basalaev *et al.*[58] while there is some agreement of our results with theirs, there are some disagreements particularly at higher frequencies.

TABLE VIII. Top table lists lattice parameters (in Å) for the $C2/c$ structure of α-P_3N_5 comparing calculated results with the experimental results of Ref. 24. Second table lists computed inequivalent fractional coordinates of a conventional of this crystal compared with the (experimental values).

	a	b	c	β (deg)
Expt.	8.12077	5.83433	9.16005	115.809
Calc.	8.14	5.85	9.17	116
Atom	Pos	x	y	z
P(1)	4e	0.000 (0.000)	0.517 (0.518)	0.750 (0.750)
P(2)	8f	0.135 (0.136)	0.204 (0.204)	0.056 (0.057)
N(1)	4a	0.000 (0.000)	0.000 (0.000)	0.000 (0.000)
N(2)	8f	0.132 (0.129)	0.362 (0.362)	0.192 (0.192)
N(3)	8f	0.145 (0.143)	0.355 (0.357)	−0.100(−0.101)

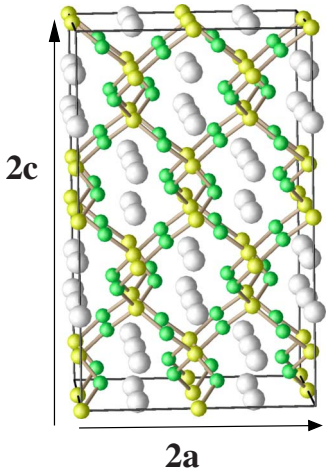

FIG. 19. (Color online) Ball and stick model of several conventional unit cells of $LiPN_2$ in the $I\bar{4}2d$ structure using the ball styles of previous diagrams.

V. DISCUSSION AND SUMMARY

A. Predicted Li_2PO_2N structures

The prediction of several high-symmetry stable crystals having the composition of Li_2PO_2N is very intriguing. To the best of our knowledge, these structures have not been yet realized experimentally. However, from the calculations of heats of formation, we can predict several possible exothermic reactions that could produce s_1-Li_2PO_2N or s_2-Li_2PO_2N. Some of these are listed in Table XI below.

TABLE IX. Structural parameters of $LiPN_2$ in the $I\bar{4}2d$ structure, comparing calculated results with the experimental results of Ref. 52. For this structure, the inequivalent atomic positions are Li at 4b sites $(0,0,\frac{1}{2})$, P at 4a sites (0,0,0), and N at 8d sites $(x,\frac{1}{4},\frac{1}{8})$. The table lists lattice constants (in Å) and x.

	a	c	x
Expt.	4.575	7.118	0.1699
Calc.	4.47	7.26	0.173

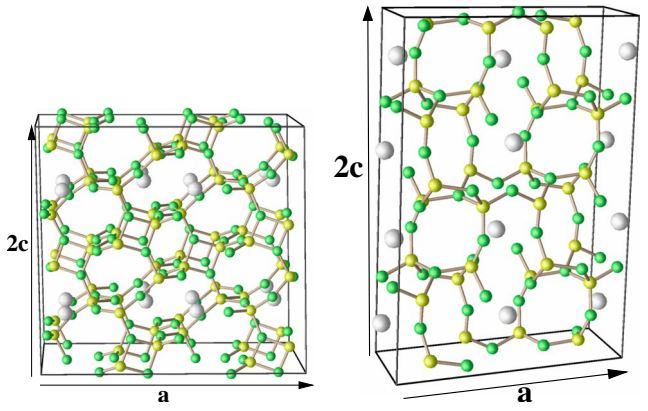

FIG. 20. (Color online) Ball and stick models of multiple conventional cells of LiP_4N_7 using the ball styles of previous diagrams. The (a) diagram shows the $P2_1/c$ structure using the conventions of Ref. 25 and the (b) diagram shows $C2/c$ structure using the conventions of Ref. 26.

From the viewpoint of testing the predictive capabilities of first-principles calculations, we would like to challenge our experimental colleagues to study some of these reactions as well as others. The fact that Li_2PO_2N has not been reported in the literature may indicate that the computer models are incorrect but it may also be simply that *no experimental study has yet included the conditions which would allow* Li_2PO_2N to be produced. For example, in their study of glassy LiNaPON materials, Le Sauze *et al.*[61] used the composition range $Li_{0.5}Na_{0.5}PO_{3-3x/2}N_x$, with $0<x\leq 0.55$. By keeping the $Li_{0.5}Na_{0.5}$ concentration constant, it would not have been possible to reach the equivalent stoichiometry of $LiNaPO_2N$.

Our preliminary results on the electrolyte properties of Li_2PO_2N indicate that activation energies for Li-ion conduction are similar to that of natural $LiPO_3$. While Li_2PO_2N may or may not turn out to be technologically useful as an electrolyte, it will at least provide a valuable reference material for unraveling the properties of the LiPON family of electrolytes.

B. Triply coordinated N in LiPON materials

There is considerable experimental evidence that N content in disordered oxynitride and phosphorus oxynitride materials improves the mechanical and chemical properties of the material in terms of increased chemical stability and physical hardness and decreasing the thermal-expansion coefficient.[62] As a possible mechanism for the stabilizing effects of N, the literature on LiPON films has many references to doubly and triply coordinated N sites.[4,22,61,63] In addition to their stability, the electrolyte properties of these materials are also of interest which means that they should also contain mobile Li ions. At the extreme concentration of triply coordinated N exhibited by α-P_3N_5, there are no mobile Li ions. The two possible forms of LiP_4O_7 that we have analyzed have a small concentration of mobile Li ions and some triply coordinated N sites. Thus for crystalline forms of LiPON materials, it seems that triply coordinated N materials can only occur at low Li concentrations. The structural conditions of disordered thin films are of course less restrictive

TABLE X. Lattice parameters (in Å) for metastable structures of LiP_4PN_7 compared with corresponding experimental structures of HP_4PN_7 ($P2_1/c$ Ref. 25) and NaP_4PN_7 ($C2/c$ Ref. 26).

		a	b	c	β (deg)
$P2_1/c$	Expt.	15.0795	4.80304	7.10722	92.191
$P2_1/c$	Calc.	15.09	4.86	7.06	91
$C2/c$	Expt.	12.3345	8.5230	5.1397	102.572
$C2/c$	Calc.	11.77	8.26	5.10	102

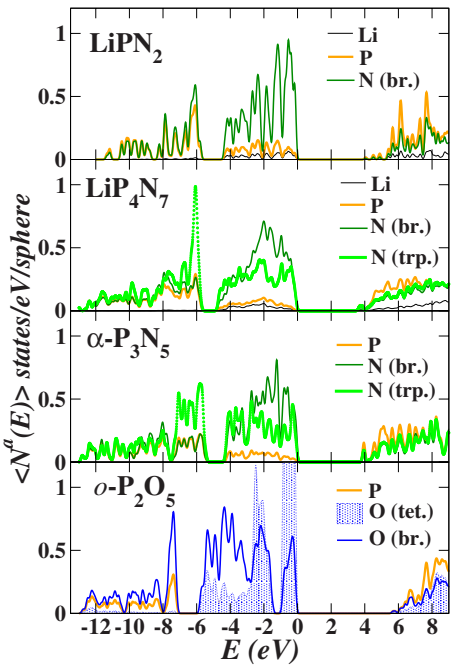

FIG. 21. (Color online) Partial densities of states of some network structured materials. The notation is similar to that used in previous diagrams with the addition of "(trp.)" to indicate triply coordinated N site contributions.

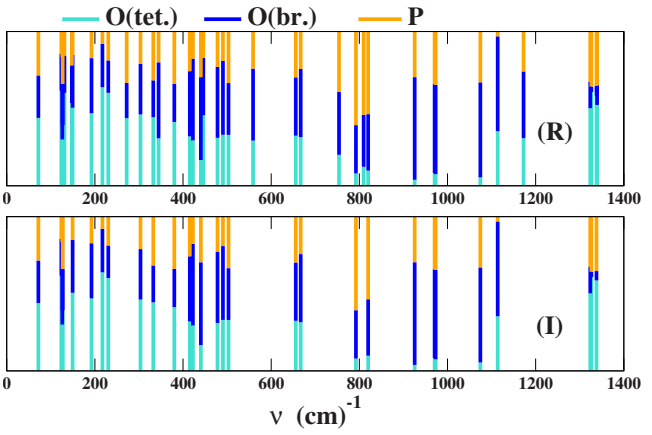

FIG. 22. (Color online) Raman-active (R) and infrared-active (I) zone-center lattice vibrations for o-P_2O_5 using scheme of previous diagrams.

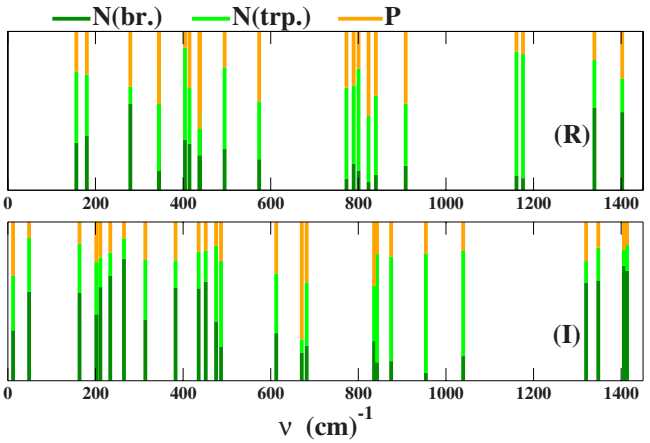

FIG. 23. (Color online) Raman-active (R) and infrared-active (I) zone-center lattice vibrations for α-P_3N_5 using scheme of previous diagrams with the addition of the notation (trp.) to indicate triply coordinated N amplitudes.

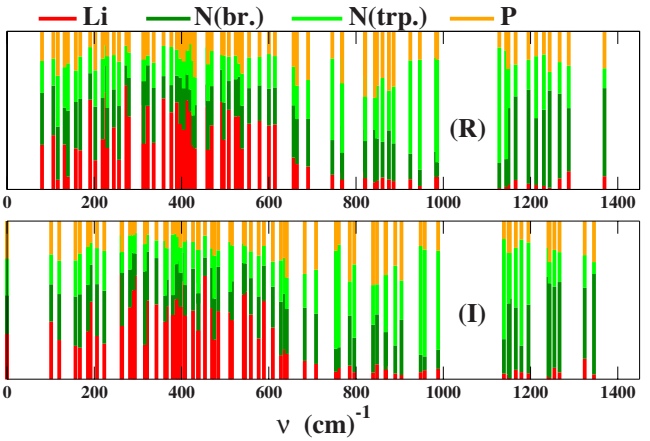

FIG. 25. (Color online) Raman-active (R) and infrared-active (I) zone-center lattice vibrations for LiP_4N_7 in the $P2_1/c$ structure using scheme of previous diagrams.

that those of the crystal but this reasoning leads to the suggestion that in order to sustain the Li concentrations of typical LiPON films, only a small number of triply coordinated N sites are possible. Here we have defined a triply coordinated N site to refer to a N which is bonded to 3 P's whereas the experimental detection of triply coordinated N sites may be more general. For example, in the s_1-Li_2PO_2N and s_2-Li_2PO_2N structures, the N's are each bonded to two phosphate groups but they are also each positioned close to a Li site as well. If this would be detected as a triply coordinated N site, it seems conceivable that s_1-Li_2PO_2N-like structures might be present in small regions of LiPON films.

The experimental detection of triply coordinated N sites, as well as other bonding configurations has used x-ray absorption, nuclear magnetic resonance, and vibrational spectroscopy.[4,22,61,63] In terms of the vibrational spectroscopy, we see that it is difficult to identify "signature" vibrational modes associated with N sites or with other components of the system. For example, by comparing the Raman spectra $Li_4P_2O_7$ and $Li_5P_2O_6N$ in Figs. 4 and 5, we see that one of the modes involving the bridging O and N sites has a frequency of 920 cm^{-1} in $Li_4P_2O_7$ and 780 cm^{-1} in $Li_5P_2O_6N$. Since we have not yet analyzed the amplitudes of these spectra, more work needs to be done. On the other hand, it is clear that the phonon spectra are not localized probes of the structure. For example, the bridge-bonding N contribution which is found at the frequency 780 cm^{-1} in the dimer material $Li_5P_2O_6N$ is found at frequency 850 cm^{-1} in the infinite chain material s_1-Li_2PO_2N. The modes associated with bond stretching of the tetrahedral P-O bonds are also not invariant to the other structural properties of these materials. The same argument applies to identify modes associated with the triply coordinated N sites in α-P_3N_5 or LiP_4N_7. On the other hand, it is clear that, if vibrational spectra of a material are available, calculations such as those reported here can be helpful for analyzing possible structural forms.

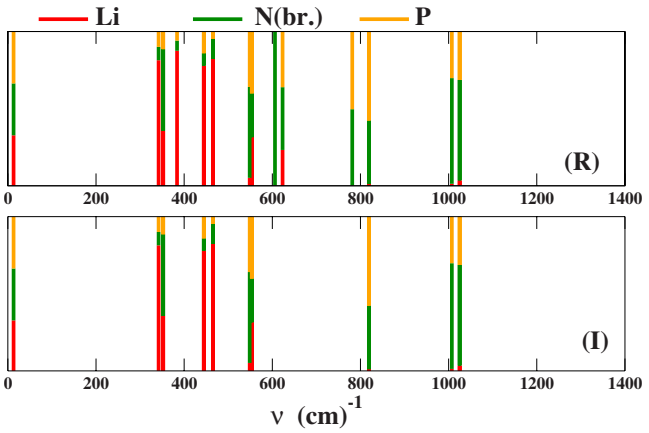

FIG. 24. (Color online) Raman-active (R) and infrared-active (I) zone-center lattice vibrations for $LiPN_2$ using scheme of previous diagrams.

C. Summary

In this paper, we have presented a comprehensive survey of crystalline members of the LiPON family, including both known and predicted materials. Having demonstrated reasonably good agreement with experimental measurements of

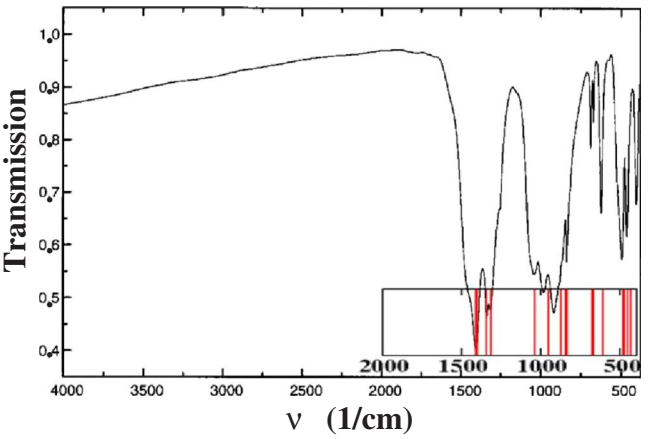

FIG. 26. (Color online) Infrared spectrum of α-P_3N_5 reproduced from Ref. 24 and superposed with the corresponding frequencies calculated in this work (also shown in Fig. 23).

TABLE XI. Some predicted reactions to produce s_1-Li_2PO_2N or s_2-Li_2PO_2N with ΔH in electron volts indicating the predicted exothermic energy release as in Table II.

Reaction	ΔH
$\frac{1}{5}P_2O_5+\frac{1}{5}P_3N_5 \rightarrow Li_2PO_2N$	2.5
$LiPO_3+Li_3N \rightarrow Li_2PO_2N+Li_2O$	4.5
$LiNO_3+Li+P \rightarrow Li_2PO_2N+\frac{1}{2}O_2$	7.0

some structural parameters, heats of formation, and lattice vibrational spectra, we have some confidence in the accuracy of our results. We hope that as new structural analyses, calorimetry, and vibrational spectroscopy measurements of these materials become available, they will be used to refine this database both for the purpose of better understanding this interesting family of materials and for the purpose of testing the capabilities of first-principles calculations. We are particularly excited about the prediction of the new materials s_1-Li_2PO_2N and s_2-Li_2PO_2N. It will be very interesting to see if they can be physically realized.

ACKNOWLEDGMENTS

This work was supported by NSF under Grants No. DMR-0427055 and No. DMR-0705239. We would also like to thank G. Lopez for performing calculations on black phosphorus; N. Lepley for performing calculations on Li_2PO_2N; R. Noftle, A. Lachgar, and R. Williams for helpful discussions; and G. Holzwarth and B. Kolb for Matlab help. Computations were performed on the Wake Forest University DEAC cluster, a centrally managed resource with support provided in part by the University.

APPENDIX: ADDITIONAL STRUCTURAL TABLES

We present here some of the longer structural tables mentioned in the body of the paper.

TABLE XII. Computed inequivalent fractional coordinates of a conventional cell of the $P\bar{1}$ structure of $Li_5P_2O_6N$, using atomic labels consistent with $Li_4P_2O_7$ described in Table III.

Atom	x	y	z
P(1)	0.830	0.208	0.422
P(2)	0.637	−0.193	0.218
N(1)	0.673	0.042	0.245
O(2)	0.843	0.223	0.747
O(3)	0.791	0.406	0.402
O(4)	0.986	0.154	0.279
O(5)	0.638	−0.213	0.528
O(6)	0.468	−0.281	0.059
O(7)	0.768	−0.301	0.048
Li(1)	0.806	0.676	0.643
Li(2)	0.442	0.716	0.673
Li(3)	0.754	0.430	0.020
Li(4)	0.984	0.862	0.121
Li(5)	−0.346	0.055	−0.175

TABLE XIII. Computed inequivalent fractional coordinates of a conventional cell of $LiPO_3$ in the $P2/c$ structure compared with (experimental values) reported in Ref. 20. The Pos column gives the multiplicity and Wyckoff label (Ref. 43).

Site	Pos	x	y	z
P(1)	4g	0.453 (0.452)	0.678 (0.673)	0.319 (0.317)
P(2)	4g	0.351 (0.352)	0.337 (0.340)	0.418 (0.417)
P(3)	4g	0.236 (0.239)	0.695 (0.688)	0.510 (0.509)
P(4)	4g	0.124 (0.126)	0.344 (0.345)	0.603 (0.602)
P(5)	4g	0.032 (0.033)	0.694 (0.688)	0.708 (0.706)
O(1)	4g	0.357 (0.359)	0.756 (0.756)	0.262 (0.261)
O(2)	4g	0.542 (0.541)	0.855 (0.844)	0.339 (0.339)
O(3)	4g	0.492 (0.494)	0.412 (0.416)	0.289 (0.286)
O(4)	4g	0.419 (0.422)	0.584 (0.577)	0.405 (0.402)
O(5)	4g	0.423 (0.423)	0.135 (0.145)	0.455 (0.454)
O(6)	4g	0.278 (0.280)	0.283 (0.283)	0.340 (0.341)
O(7)	4g	0.289 (0.295)	0.433 (0.436)	0.489 (0.488)
O(8)	4g	0.310 (0.310)	0.826 (0.819)	0.576 (0.573)
O(9)	4g	0.193 (0.194)	0.833 (0.826)	0.433 (0.435)
O(10)	4g	0.138 (0.143)	0.589 (0.584)	0.548 (0.547)
O(11)	4g	0.076 (0.076)	0.138 (0.150)	0.548 (0.548)
O(12)	4g	0.222 (0.221)	0.299 (0.296)	0.662 (0.659)
O(13)	4g	0.035 (0.036)	0.442 (0.445)	0.653 (0.651)
O(14)	4g	0.142 (0.139)	0.787 (0.779)	0.733 (0.731)
O(15)	4g	−0.049(−0.047)	0.865 (0.859)	0.664 (0.663)
Li(1)	4g	0.182 (0.184)	−0.006(−0.010)	0.326 (0.325)
Li(2)	4g	0.321 (0.323)	0.025 (0.021)	0.675 (0.674)
Li(3)	4g	−0.060(−0.061)	1.009 (0.999)	0.558 (0.558)
Li(4)	4g	0.560 (0.558)	0.035 (0.020)	0.442 (0.442)
Li(5)	2f	0.250 (0.250)	0.508 (0.504)	0.250 (0.250)
Li(6)	2f	0.250 (0.250)	0.544 (0.535)	0.750 (0.750)

TABLE XIV. Computed inequivalent conventional cell fractional coordinates for the $Pmc2_1$ structures of s_3-Li_2PO_2N and s_3-$LiPO_3$.

Atom	Pos	x	y	z
		s_3-Li_2PO_2N		
Li(1)	4c	0.252	−0.468	0.349
Li(2)	2b	0.500	−0.006	0.229
Li(3)	2a	0.000	0.267	0.091
P(1)	2a	0.000	−0.238	0.081
P(2)	2b	0.500	0.042	0.474
O(1)	2b	0.500	−0.211	0.390
O(2)	2b	0.500	0.260	0.368
O(3)	2a	0.000	−0.400	0.212
O(4)	2a	0.000	0.447	0.471
N	4c	−0.250	−0.045	0.074
		s_3-$LiPO_3$		
Li	4c	0.250	−0.402	0.361
P(1)	2a	0.000	−0.286	0.083
P(2)	2b	0.500	0.102	0.453
O(1)	2b	0.500	−0.148	0.388
O(2)	2b	0.500	0.333	0.370
O(3)	2a	0.000	−0.337	0.228
O(4)	2a	0.000	0.501	0.489
O(5)	4c	−0.250	−0.107	0.053

TABLE XV. Computed inequivalent fractional coordinates of a conventional cell for the $P2_1/c$ structure of LiP_4N_7 compared with the experimental values (in parentheses) of HP_4N_7 from Ref. 25, except for the H positions which are unknown.

Atom	Pos	x	y	z
Li	4e	0.095	0.186	0.480
P(1)	4e	0.451 (0.445)	0.197 (0.198)	0.761 (0.760)
P(2)	4e	0.701 (0.701)	−0.143(−0.126)	0.954 (0.953)
P(3)	4e	0.302 (0.304)	0.180 (0.191)	0.482 (0.482)
P(4)	4e	0.556 (0.557)	−0.304(−0.305)	0.805 (0.805)
N(1)	4e	0.658 (0.657)	−0.219(−0.222)	0.738 (0.741)
N(2)	4e	0.540 (0.538)	0.379 (0.374)	0.764 (0.784)
N(3)	4e	0.476 (0.474)	−0.122(−0.127)	0.726 (0.722)
N(4)	4e	0.382 (0.382)	0.303 (0.307)	0.607 (0.609)
N(5)	4e	0.287 (0.284)	−0.142(−0.144)	0.510 (0.521)
N(6)	4e	0.779 (0.782)	−0.327(−0.283)	0.026 (0.032)
N(7)	4e	0.404 (0.402)	0.226 (0.212)	0.974 (0.976)

TABLE XVI. Computed inequivalent fractional coordinates of a conventional cell for the $C2/c$ structure of LiP_4N_7 compared with the experimental values (in parentheses) of NaP_4N_7 from Ref. 26, assuming Li occupies the Na sites.

Atom	Pos	x	y	z
Li	4e	0.000 (0.000)	0.217 (0.211)	0.250 (0.250)
P(1)	8f	0.341 (0.330)	0.425 (0.426)	0.175 (0.197)
P(2)	8f	0.377 (0.376)	0.075 (0.078)	0.229 (0.205)
N(1)	4e	0.000 (0.000)	0.491 (0.522)	0.250 (0.250)
N(2)	8f	0.118 (0.135)	0.067 (0.050)	0.107 (0.073)
N(3)	8f	0.373 (0.360)	0.256 (0.247)	0.322 (0.392)
N(4)	8f	0.193 (0.185)	0.456 (0.449)	0.086 (0.116)

*Present address: ICAMS, Ruhr-Universität, 44780 Bochum, Germany.
†Corresponding author; natalie@wfu.edu; http://www.wfu.edu/~natalie

[1] N. J. Dudney, Interface **17** (3), 44 (2008).
[2] J. B. Bates, N. J. Dudney, B. Neudecker, A. Ueda, and C. D. Evans, Solid State Ion. **135**, 33 (2000).
[3] X. Yu, J. B. Bates, J. G. E. Jellison, and F. X. Hart, J. Electrochem. Soc. **144**, 524 (1997).
[4] B. Wang, B. C. Chakoumakos, B. C. Sales, B. S. Kwak, and J. B. Bates, J. Solid State Chem. **115**, 313 (1995).
[5] J. B. Bates, N. J. Dudney, D. C. Lubben, G. R. Gruzalski, B. S. Kwak, X. Yu, and R. A. Zuhr, J. Power Sources **54**, 58 (1995).
[6] B. Wang, B. S. Kwak, B. C. Sales, and J. B. Bates, J. Non-Cryst. Solids **183**, 297 (1995).
[7] J. B. Bates, G. R. Gruzalski, N. J. Dudney, C. F. Luck, and X. Yu, Solid State Ion. **70-71**, 619 (1994).
[8] J. B. Bates, N. J. Dudney, G. R. Gruzalski, R. A. Zuhr, A. Choudhury, D. F. Luck, and J. D. Robertson, J. Power Sources **43**, 103 (1993).
[9] J. B. Bates, N. J. Dudney, G. R. Gruzalski, R. A. Zuhr, A. Choudhury, D. F. Luck, and J. D. Robertson, Solid State Ion. **53-56**, 647 (1992).
[10] A. Patil, V. Patil, D. W. Shin, J.-W. Choi, D.-S. Paik, and S.-J. Yoon, Mater. Res. Bull. **43**, 1913 (2008).
[11] Y. G. Kim and H. Wadley, J. Power Sources **187**, 591 (2009).
[12] F. Muñoz, A. Durán, L. Pascual, L. Montagne, B. Revel, and A. C. M. Rodrigues, Solid State Ion. **179**, 574 (2008).
[13] Y. Hamon, A. Douard, F. Sabary, C. Marcel, P. Vinatier, B. Pecquenard, and A. Levasseur, Solid State Ion. **177**, 257 (2006).
[14] H. Y. Park, S. C. Ham, Y. C. Lim, K. G. Choi, K. C. Lee, G. B. Park, S.-R. L. H. P. Kim, and S. B. Cho, J. Electroceram. **17**, 1023 (2006).
[15] F. N. Rhines, *Phase Diagrams in Metallurgy* (McGraw-Hill, New York, 1956).
[16] O. V. Yakubovich and V. S. Urusov, Crystallogr. Rep. **42**, 261 (1997).
[17] W. Schnick and J. Luecke, J. Solid State Chem. **87**, 101 (1990).
[18] A. Daidouh, M. L. Veiga, C. Pico, and M. Martinez-Ripoll, Acta Crystallogr., Sect. C: Cryst. Struct. Commun. **53**, 167 (1997).
[19] J. C. Guitel and I. Tordjman, Acta Cryst. B **32**, 2960 (1976), note: we found a typo in the fractional coordinates reported in Table I. Oxygen position OE10B given as (0.5575, 0.3243, 0.6795) should be approximately (0.5575, 0.3243, 0.0052).
[20] E. V. Murashova and N. N. Chudinova, Crystallogr. Rep. **46**, 942 (2001).
[21] E. H. Arbib, B. Elouadi, J. P. Chaminade, and J. Darriet, J. Solid State Chem. **127**, 350 (1996).
[22] B. C. Bunker, D. R. Tallant, C. A. Balfe, R. J. Kirkpatrick, G. L. Turner, and M. R. Reidmeyer, J. Am. Ceram. Soc. **70**, 675 (1987).
[23] R. Marchand, P. L'Haridon, and Y. Laurent, J. Solid State Chem. **43**, 126 (1982).
[24] S. Horstmann, E. Irran, and W. Schnick, Z. Anorg. Allg. Chem. **624**, 620 (1998).
[25] S. Horstmann, E. Irran, and W. Schnick, Z. Anorg. Allg. Chem. **624**, 221 (1998).
[26] K. Landskron, E. Irran, and W. Schnick, Chem.-Eur. J. **5**, 2548 (1999).
[27] Y. A. Du and N. A. W. Holzwarth, Phys. Rev. B **78**, 174301 (2008).
[28] Y. A. Du and N. A. W. Holzwarth, Phys. Rev. B **76**, 174302

(2007).
[29] Y. A. Du and N. A. W. Holzwarth, J. Electrochem. Soc. **154**, A999 (2007).
[30] P. Hohenberg and W. Kohn, Phys. Rev. **136**, B864 (1964).
[31] W. Kohn and L. J. Sham, Phys. Rev. **140**, A1133 (1965).
[32] P. Giannozzi *et al.*, J. Phys.: Condens. Matter **21**, 395502 (2009), available from the website http://www.quantum-espresso.org.
[33] D. Vanderbilt, Phys. Rev. B **41**, 7892 (1990), USPP code is available from the website http://www.physics.rutgers.edu/~dhv/uspp/.
[34] P. Tang, Ph.D. thesis, Wake Forest University, 2006.
[35] P. Tang, N. A. W. Holzwarth, and Y. A. Du, Phys. Rev. B **76**, 174118 (2007).
[36] J. P. Perdew and Y. Wang, Phys. Rev. B **45**, 13244 (1992).
[37] N. A. W. Holzwarth, A. R. Tackett, and G. E. Matthews, Comput. Phys. Commun. **135**, 329 (2001) available from the website http://pwpaw.wfu.edu.
[38] A. R. Tackett, N. A. W. Holzwarth, and G. E. Matthews, Comput. Phys. Commun. **135**, 348 (2001) available from the website http://pwpaw.wfu.edu.
[39] P. E. Blöchl, Phys. Rev. B **50**, 17953 (1994).
[40] M. Torrent, F. Jollet, F. Bottin, G. Zérah, and X. Gonze, Comput. Mater. Sci. **42**, 337 (2008), available from the website http://www.abinit.org.
[41] *CRC Handbook of Chemistry and Physics*, 90th ed., edited by D. R. Lide (CRC Press, Boca Raton/Taylor & Francis, London, 2009).
[42] W. A. Crichton, M. Mezouar, G. Monaco, and S. Falconi, Powder Diffr. **18**, 155 (2003).
[43] *International Tables for Crystallography*, Space-Group Symmetry Vol. A, 5th revised edition, edited by T. Hahn (Kluwer, Dordrecht, 2002).
[44] L. Wang, T. Maxisch, and G. Ceder, Phys. Rev. B **73**, 195107 (2006).
[45] Database maintained at the National Institute of Standards and Techology (NIST) website (http://webbook.nist.gov/).
[46] W. S. Holmes, Trans. Faraday Soc. **58**, 1916 (1962).
[47] Estimated from ΔH of hexagonal form and the transformation energy to the octahedral form given in Table 12.5 in N. N. Greenwood and A. Earnshaw, *Chemistry of the Elements*, 2nd ed. (Butterworth-Heinemann, Amsterdam, 1997).
[48] F. Tessier and A. Navrotsky, Chem. Mater. **12**, 148 (2000).
[49] X. Wu, F. R. Fronczek, and L. G. Butler, Inorg. Chem. **33**, 1363 (1994).
[50] M. Jansen and B. Lüer, Z. Kristallogr. **177**, 149 (1986).
[51] J. M. Léger, J. Haines, C. Chateau, G. Bocquillon, M. W. Schmidt, S. Hull, F. Gorelli, A. Le Sauze, and R. Marchand, Phys. Chem. Miner. **28**, 388 (2001).
[52] W. Schnick and J. Lücke, Z. Anorg. Allg. Chem. **588**, 19 (1990).
[53] B. K. Money and K. Hariharan, Appl. Phys. A **88**, 647 (2007).
[54] R. Marchand, W. Schnick, and N. Stock, Adv. Inorg. Chem. **50**, 193 (2000).
[55] C. A. Coulson, *Valence* (Clarendon Press, Oxford, 1952), p. 106.
[56] P. Kroll and W. Schnick, Chem.-Eur. J. **8**, 3530 (2002).
[57] J. Dong, A. A. Kinkhabwala, and P. F. McMillan, Phys. Status Solidi B **241**, 2319 (2004).
[58] Y. M. Basalaev, A. V. Kosobutsky, and A. S. Poplavnoi, Semiconductors **43**, 735 (2009).
[59] W. Schnick, J. Lücke, and F. Krumeich, Chem. Mater. **8**, 281 (1996).
[60] In Ref. 56, we believe there is a small typo in the symmetry decomposition of the zone-center phonons. We believe the correct decomposition should read $\Gamma_{opt}=10A_g+12A_u+11B_g+12B_u$ instead of $\Gamma_{opt}=10A_g+10A_u+11B_g+14B_u$.
[61] A. Le Sauze and R. Marchand, J. Non-Cryst. Solids **263-264**, 285 (2000).
[62] M. R. Reidmeyer and D. E. Day, J. Non-Cryst. Solids **181**, 201 (1995).
[63] F. Münoz, L. Pascual, A. Durdan, J. Rocherulle, and R. Marchand, Silic. Ind. **69**, 105 (2004).